Hindawi
International Journal of Energy Research
Volume 2024, Article ID 5766655, 12 pages
https://doi.org/10.1155/2024/5766655

Research Article

Experimental Study of Condensation Heat Transfer and Droplet Dynamics on Multiple Horizontal Copper Tubes with Superhydrophobic Characteristics

Hyunjun Sun,[1] Younghun Shin,[2] Dong Kyou Park,[3] and Kwon-Yeong Lee[1]

[1]*Department of Mechanical and Control Engineering, Handong Global University, Pohang 37554, Republic of Korea*
[2]*Department of Mechanical Engineering, Pohang University of Science and Technology (POSTECH), Pohang 37673, Republic of Korea*
[3]*Korea University of Technology and Education, 1600, Chungjeol-ro, Byeongcheon-myeon, Dongnam-gu, Cheonan-si, Chungcheongnam-do 31253, Republic of Korea*

Correspondence should be addressed to Dong Kyou Park; pdongkyou@koreatech.ac.kr
and Kwon-Yeong Lee; kylee@handong.edu

Received 7 November 2023; Revised 11 March 2024; Accepted 23 April 2024; Published 17 May 2024

Academic Editor: Guojun Yu

We conducted an experimental study on the condensation heat transfer and droplet dynamics on multiple horizontal copper tubes with superhydrophobic characteristics. Condensation heat transfer has various industrial applications such as power plants and air-conditioning systems. Because condensers are typically designed in multiple-tube configurations, studying the phenomenon of multiple tubes is important. We investigated the effect of a superhydrophobic surface modification, which induces dropwise condensation, on the heat transfer performance of multiple-tube condensers. The purpose of this research is to evaluate the extent to which heat transfer performance is improved by comparing superhydrophobic tubes with bare tubes and to analyze the impact of droplet dynamics on heat transfer performance. The results show that the heat transfer coefficient of the superhydrophobic tubes is improved by approximately 9.5%–44.9% compared to that of bare tubes. Droplet dynamic analysis revealed differences in droplet behavior between the superhydrophobic tubes and bare tubes, including the formation of droplets by condensation, the process of droplets falling on the tube surface, and the impact of droplets falling on other tubes in a multiple-tube configuration. Based on these results and observations, it can be concluded that the heat transfer performance of the superhydrophobic tube is superior to that of the bare tube. The droplet dynamic analysis demonstrated that the droplets formed on the superhydrophobic surface could be easily removed by the flow, leading to more efficient heat transfer. These findings highlight the potential for more efficient heat transfer in multiple tubes through superhydrophobic modifications.

1. Introduction

As energy problems become increasingly serious, energy efficiency has become a major concern worldwide. Sustained efforts are needed to solve the energy problem due to various causes such as population increases and energy resource depletion. To address energy issues, management and recovery of thermal energy are widely employed methods that are closely intertwined with condenser technology. Condensers play a pivotal role in various thermal machines and systems as they recover and recycle heat. In power plants and industrial facilities, condensers are instrumental in recovering heat from spent steam, cooling and compressing it, and sending it back to the boiler for reuse. Therefore, enhancing the heat transfer performance of condensers is crucial because it minimizes energy losses and enables the production of more electricity, thereby improving the thermal efficiency and ultimately enhancing the energy efficiency.

Recently, the environmental problems caused by water shortages have been highlighted. To solve the water shortage

problem, devices that collect fog and moisture from the air are being researched [1, 2]. Although research has been conducted on changing the structure of the collector to improve water collection, it is more important to improve heat transfer performance, which fundamentally affects water collection. Environmental problems must be addressed because they directly harm humans. One way to improve the performance of a condenser is to solve the energy and environmental problems simultaneously. Based on the results of the condensation experiment using humid air, it was possible to improve the condensation performance and technically improve the water collection capacity.

Condensation is classified into two types according to wettability: film condensation and dropwise condensation [3]. When condensation occurs, dropwise condensation initially occurs. However, as the droplet grows, it undergoes changes to film condensation. Film condensation occurs in almost all the condensers. During film condensation, a continuous liquid film is formed, and heat must pass through this film to exchange the surface heat. Because this film provides thermal resistance, it reduces the heat transfer performance [4, 5]. Unlike film condensation, dropwise condensation does not continuously form a liquid film. Because there is less thermal resistance owing to the liquid film, dropwise condensation has better condensation heat transfer performance than film condensation [6]. Therefore, if dropwise condensation is maintained, efficiency can be improved. The characterization of dropwise condensation has also been tried using computational fluid dynamics (CFD) [7]. The presence of noncondensable gases adversely affects the efficiency of condensation. Consequently, efforts have been made to minimize the impact of noncondensable gases to enhance performance [8].

The condensation type is influenced by thermophysical parameters, surface properties (structure and material), and condensation characteristics. Surface modification can promote dropwise condensation by coating the surface, changing the material, or changing the structural properties of the surface [9, 10]. Methods to increase the condensation surface area by altering structural properties, such as micro V-grooves, square grooves, and 3D hybrid surfaces, have been investigated [11–13]. Various methods have been proposed using micro/nanostructured surfaces that can lower the surface energy such that the droplets can be easily detached from the surface [14, 15].

Liao et al. [16] conducted a study to improve the heat transfer coefficient by 13.9% using a silicon wafer-based surface. Rausch et al. [17] improved the heat transfer coefficient by 18% using an ion-implanted aluminum surface, and Miljkovic et al. [18] improved the heat transfer coefficient by 20% using a functionalized CuO nanostructure coating. Lee et al. [19] improved the heat transfer coefficient by 25% through a polymer coating. In addition to the aforementioned studies, attempts have been made to improve the heat transfer performance through various types of surface modifications [20, 21]. The stable performance of heat transfer was enhanced through the application of coatings, achieved using materials such as polytetrafluoroethylene (PTFE) film and various polymers [22, 23]. Among the surface coating technologies, superhydrophobic surface modification using self-assembled monolayers (SAMs) has been researched. SAM coatings are very thin and uniform which is advantageous for heat transfer [24]. The main advantage is the creation of a smooth solid surface by forming a protective hydrophobic layer that offers negligible heat transfer resistance [25]. Marto et al. [26] used SAM on gold and copper surfaces and observed contact angles greater than 100°. Chen et al. [27] demonstrated that the heat transfer performance was improved about 1.7 to 2.1 times in dropwise condensation using a SAM compared to film condensation that occurred on a bare surface in a single tube.

Most surface-modified condensation experiments, including the aforementioned studies, are single-tube experiments [28–31]. Although the single-tube experiment has the advantage of confirming the improvement in the heat transfer performance according to the presence or absence of surface modification, the condenser is composed of multiple tubes to increase the heat transfer capacity. Therefore, it is essential to study the condensation phenomenon in a tube bundle because various factors affect heat transfer performance. Makas [32] presented the analytical and experimental methods for film condensation in multiple horizontal tubes. As for multiple-tube condensation research, efforts have been made to improve the heat transfer performance through the distance between tubes, the presence or absence of fins, and the shape deformation of the tube; however, most multiple-tube research focuses on film condensation for practicality [33–35]. A multiple-tube dropwise condensation heat transfer experiment involving surface modification was also conducted. Zhu et al. [36] demonstrated that the condensation performance can be improved by inserting plasma ions into horizontal tube bundles. In addition, a heat transfer analysis was performed with and without a hydrophobic coating along with a fin in the tube bundle [37]. However, tube bundle condensation experiments employing SAM coatings are rare.

Droplet dynamics have rarely been investigated. The heat transfer of dropwise condensation reached a maximum at the beginning of condensation. As the droplets grow, the heat flux gradually decreases, but when the droplets fall, the heat flux reaches a high point [38]. Therefore, making droplets fall frequently is one way to realize continuous dropwise condensation and improve surface heat transfer. To analyze this phenomenon, it was necessary to observe the droplet behavior between the tubes. Droplet dynamics play an important role in the heat transfer of tube bundles. Because heat transfer performance is greatly influenced by droplet dynamics, visual experiments are required to observe droplet behavior. Therefore, the heat transfer performance can be evaluated more accurately through droplet behavior analysis in multiple tubes. Several studies have been conducted on condensation heat transfer based on droplet behavior. Nakajima [39] demonstrated that the droplet behavior differs depending on the surface, and Patil et al. [40] experimentally verified that surface modification affects the droplet bounce amount and distance when it falls on a flat plate. In addition, Liu et al. [41] analyzed the effect of pancake bouncing on hydrophobic surfaces according to

the slope. Lee et al. [42] observed droplet flow through a modified surface and suggested the point at which the droplet behavior changed significantly, which had a significant effect on heat transfer. However, studies on droplet behavior have mainly been conducted in single tubes, similar to surface-modified condensation experiments [43]. However, to observe the droplet behavior between tubes, the behavior of multiple-tube droplets must be studied. Therefore, it is necessary to study droplet behavior when applied to multiple tubes with a hydrophobic coating and how the droplet interacts with the tubes.

Therefore, a new experimental facility was designed to analyze the heat transfer performance by easily observing the droplet dynamics in a multiple-tube condensation situation and calculating the condensation heat transfer coefficient of each tube. In this study, we compared the condensation performance of a superhydrophobic (SAM-coated surface) copper tube with a nanosized surface structure and a bare tube in multiple horizontal tubes using humid air and observed the droplet behavior. In this study, we analyzed the causes of the improved heat transfer performance and their interactions in multiple tubes.

2. Experiment

2.1. Superhydrophobic Surface Modification and Contact Angle Measurement. Superhydrophobicity, a phenomenon where surfaces exhibit extreme water repellence, is primarily achieved through a combination of surface roughness at the micro- and nanoscale and low surface energy. The micro/nanosurface structure introduces air pockets between the water droplet and the surface, significantly reducing the area of contact. This roughness amplifies the inherent water-repellent properties of materials with low surface energy, leading to the formation of nearly spherical droplets that easily roll off the surface [44]. Zhong et al. [45] fabricated superhydrophobic surfaces with a contact angle of 148 degrees through microposts and microgrooves. Neumann et al. [46] demonstrated that the decrease in contact angle hysteresis on an inclined plane correlates with an increase in the heat transfer coefficient and heat flux. Furthermore, they provided evidence that an increase in the advancing contact angle is associated with a concurrent rise in these parameters. In this study, the reduction of surface energy to achieve superhydrophobicity was accomplished through the use of self-assembled monolayers (SAMs). SAMs are molecular assemblies that spontaneously form on surfaces, creating a uniform and stable coating with tailored chemical properties. Three processes were performed to create superhydrophobicity on the tube surfaces. First, sonication was performed for 30 min using ethanol to remove the naturally occurring oxide layer and impurities from the surface of the copper tube. Second, to implement a nanostructured copper oxide layer on the surface, we dissolved sodium hydroxide (2.5 M, 100 g/l) and ammonium persulfate (0.2 M, 45.64 g/l) in deionized water, maintaining the solution at 4°C for 1 hour to optimize the oxidation process of copper tubes. This temperature was specifically chosen because water's maximum density at 4°C improves particle suspension, ensuring uniform distribution essential for consistent chemical reactions. Additionally, the lower vapor pressure at this temperature reduces evaporation, crucial for maintaining accurate solution concentrations. Furthermore, we dried the copper tubes in a 60°C dry oven for 30 minutes to ensure the stability of the surface. Third, to lower the surface energy, the copper tube was immersed in a 0.5 wt% n-hexane solution of 1H,1H,2H,2H-perfluorodecyltrichlorosilane (FDTS) for 1 h and dried in an oven at 60°C for 2 h. Drying was performed in a forced circulation oven, which promotes even temperature distribution. All immersion methods were performed using a setup where copper tubes were vertically immersed in the solution and stirred at 100 rpm. This arrangement facilitated uniform chemical treatment by ensuring consistent solution circulation. Through these processes, we fabricated superhydrophobic copper tubes based on nanostructures and SAM deposition. Because our method uses an immersion method, it can be applied to the surface of a tube with a curvature, and it is possible to uniformly implement superhydrophobicity even on a large-scale surface.

To confirm that the excellent superhydrophobic properties were exhibited, we measured the water contact angle of the surface. The determination of contact angles was performed using an advanced contact angle analyzer, the SmartDrop, manufactured by Femtobiomed in Korea. This device represents a significant advancement in the field of surface science, offering capabilities for simultaneous analysis of contact angle, surface tension, and surface energy. A notable feature of the SmartDrop is its versatility in applying both sessile and pendant drop methods on the same sample, which ensures consistent and reliable measurement results. Furthermore, the equipment is designed to automatically align its level upon activation or in the event of misalignment due to external forces, thereby maintaining the accuracy of measurements. For the measurements of contact angles (CAs), deionized (DI) water was chosen as the liquid. The measurement process was expedited by SmartDrop's autofitting feature, which allowed for the acquisition of a contact angle datum in less than a minute. This rapid measurement capability is crucial for minimizing environmental or operational variables. The precision of the SmartDrop is notable, offering an accuracy of ±0.1°. This high level of accuracy is intrinsic to the design and operation of the instrument, ensuring that our contact angle measurements are both precise and reliable.

To ensure the robustness of our data, we conducted five contact angle measurements at five different points on the sample surface, totaling 25 individual measurements. The results from these measurements were then averaged to determine the final contact angle values reported in our study. Addressing the potential challenges of measuring contact angles on tubular surfaces, we prepared the samples by cutting the ends of the tubes into segments with dimensions of 5 mm by 5 mm. This preparation technique allowed us to measure the contact angle on a flat surface, effectively mitigating the impact of tube curvature on the droplet shape during measurements. The size of the liquid droplet used in each measurement was standardized at 5 μl, further

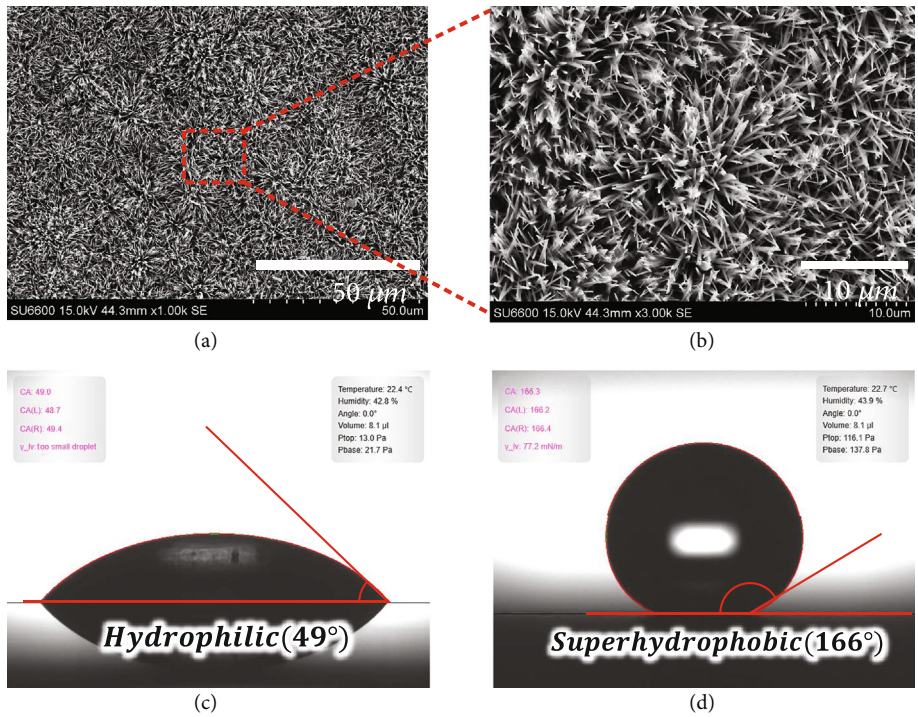

Figure 1: (a, b) SEM images of micro/nanohierarchical structure superhydrophobic copper surfaces and static contact angles of (c) bare and (d) superhydrophobic surfaces. Photograph courtesy of "Younghun Shin."

ensuring consistency across all measurements. In Figures 1(c) and 1(d), the contact angle observed on the bare copper surface is quantified at 49.4°, demonstrating hydrophilic characteristics, whereas the contact angle on the engineered superhydrophobic copper surface approximates 166.4°. These findings are underpinned by an analytical methodology where the contact angle was determined by averaging over a comprehensive set of 25 individual measurements. This analysis yielded an average contact angle of approximately 44° for the bare surface and 159° for the superhydrophobic surface. The data conclusively demonstrate the attainment of superior superhydrophobic properties, as evidenced by the contact angle measurements.

2.2. Experimental Facility. The experimental facility for multiple horizontal tube condensation experiments is shown in Figure 2. The design goal was to create a facility that requires minimal space and allows for easy observation of droplet dynamics during condensation. A TEC (thermal electric cooler) cooling device is used to control the temperature of the tube. The model used was TEC1-12712 with a maximum operating current of 12 A and dimensions of 40 mm × 40 mm × 3.6 mm. Each tube used in the experiment was made of copper with an outer diameter of 25.4 mm, a thickness of 1 mm, and a length of 150 mm. The TEC allowed for downsizing of the experimental setup, as it has the advantage of easier control of the cooling capacity and a smaller size compared to the commonly used cooling water loop with a chiller. The inside of each tube was insulated with glass wool, and five tubes were arranged vertically with the distance between each tube set to 31.25 mm, which is 1.25 times the diameter of the tube. The temperature of the copper tube was recorded at six different locations (T1–T6) using K-type thermocouples. Totally, thirty K-type thermocouples were attached to the five tubes. Additionally, five K-type thermocouples were placed at the back of each tube to measure the bulk fluid temperature of the humid air. The thermocouples were calibrated to have ±0.15°C accuracy.

The experimental conditions are listed in Table 1. The controlled variable was the temperature value measured at T1, the first thermocouple closest to the TEC, and was maintained at 14.5°C for at least 5 minutes. The contacting surfaces between the copper tubes and the TEC were treated with Evercool's TC-200 Baikal thermal grease, which possesses a thermal conductivity of 3.8 W/m·K and a thermal impedance of 0.017, to reduce the contact resistance between the TEC and the copper tubes as well as between the copper tubes and the thermocouples. By serving as a medium to minimize thermal contact resistance, the thermal grease facilitates a more uniform temperature distribution across the contacting surfaces. This helps to compensate for any minor temperature disparities between the thermocouple and the copper tube, thereby enhancing the efficiency of heat transfer. To improve the uncertainty by increasing the temperature difference between the humidified air and tube surface, a sufficient amount of humidified air with a sufficiently high temperature was supplied by mixing the high-temperature evaporative humidifier and the low-temperature ultrasonic humidifier. The bulk fluid temperature measured with the mixed humidified air was controlled at approximately 45°C, which provided a sufficient temperature difference value to reduce uncertainty.

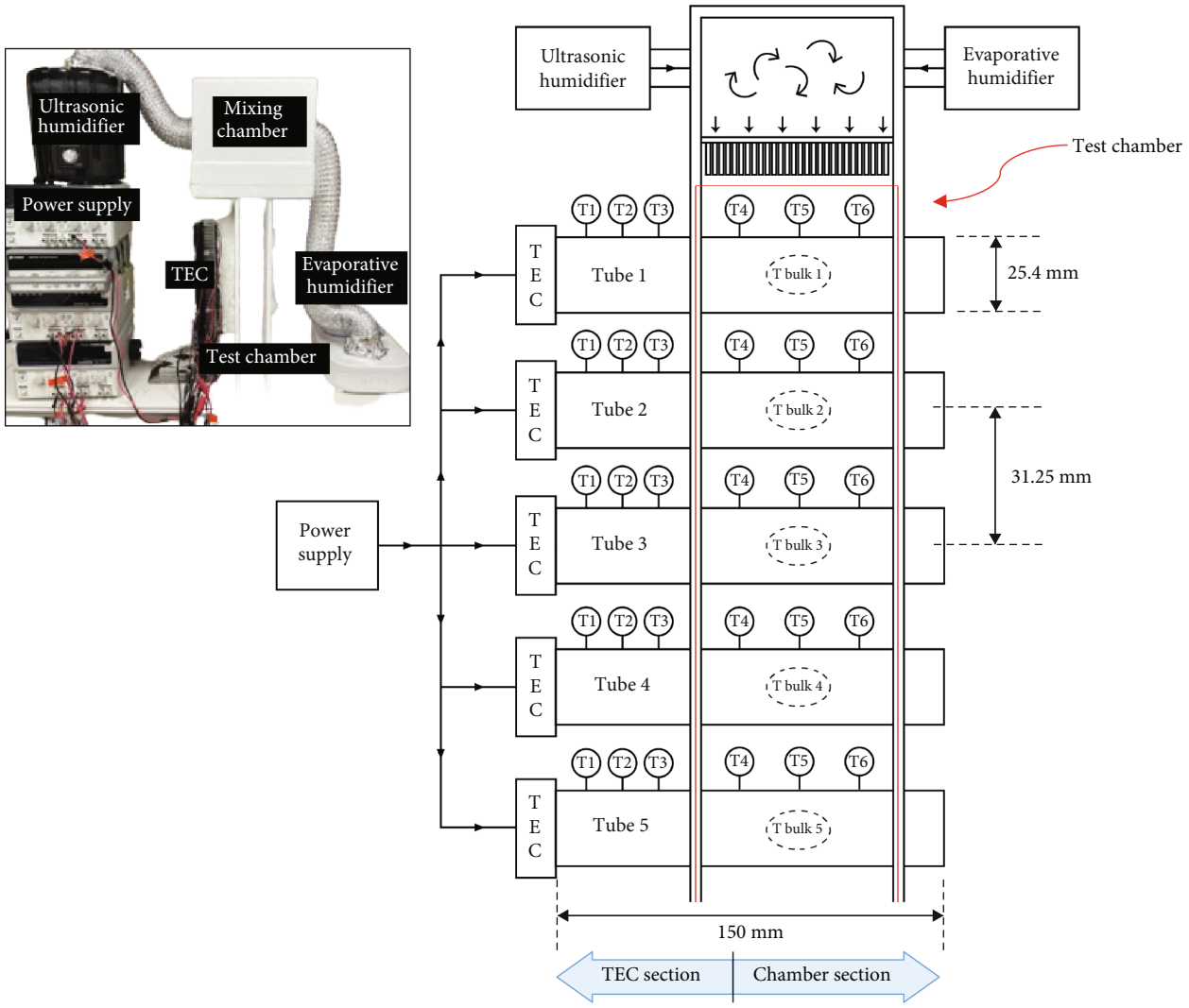

Figure 2: Experimental facility for multiple horizontal tube experiments.

Table 1: Test conditions.

Parameter	Values
Initial temperature measured at T1	14.5 (°C)
Flow rate of ultrasonic humidifier	300 ml/h
Flow rate of evaporative humidifier	400 ml/h
Temperature of mixed humidified air	42 (°C)~45 (°C)

The experiment was conducted as follows. Before starting the experiment, the surface temperature T1 through the TEC was set to the same value. Although the input power to the TEC was the same, the measured T1 values of each tube were different. So adjust each tube's temperature to be within the effective range of ±0.1°C. Once the temperature of T1 was kept constant, humidified air was supplied through an ultrasonic humidifier and a steam humidifier. A strainer consisting of multiple plastic straws was installed at the bottom of the mixing chamber to ensure that the humidified air was evenly distributed. Mixed humid air at the bottom of the mixing chamber flowed downward through the strainer into the test chamber. As the temperature of the humidified air was higher than that of the tubes, condensation occurred in the tubes. Approximately 25 min after the start of the humidified air injection, the temperature of the tubes reached a steady state. The temperature data of the tubes inside and outside the chamber were collected in a steady state, and the heat transfer coefficients of the bare and superhydrophobic tubes were calculated using the measured temperature data.

2.3. Data Reduction. Figure 3 shows a schematic of the expected temperature distribution inside the tube along the longitudinal direction. For the tubes outside the chamber (TEC section), both the inner and outer tubes were insulated; therefore, the temperature of the tubes was influenced only by the longitudinal conduction heat transfer. Therefore, it can be assumed that the temperature inside tubes T1–T3 changes linearly owing to conduction, as shown in Figure 3. However, for the tubes inside the chamber (chamber section), only the inner part of the tubes was adiabatic, and the outer tubes experienced condensation and

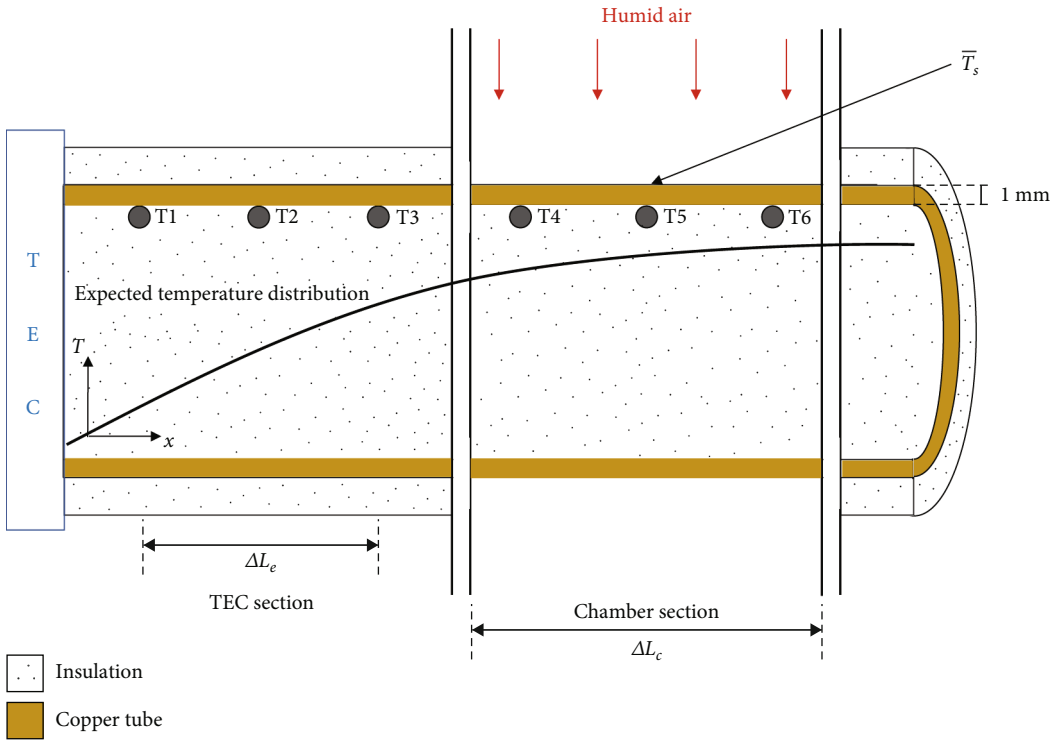

Figure 3: Schematic diagram of copper tube with a one-dimensional temperature gradient.

convection heat transfer from the humid air. Therefore, the temperatures from T4 to T6 were nearly uniform in this range, as shown in Figure 3. By insulating the tubes, we can assume that the heat transfer rate of the tubes outside the chamber $(Q_{e,\text{cond}})$ is the same as that of the tubes inside the chamber $(Q_{c,\text{cond}})$ due to energy balance equations. Furthermore, it is reasonable to assume that the heat transfer rate due to condensation and convection in the tubes inside the chamber $(Q_{c,\text{conv}})$ is the same as that due to conduction $(Q_{c,\text{cond}})$.

Figure 4 displays the temperature distribution of each thermocouple obtained from the real experiments. It can be seen that the slope (dT/dl) from T1 to T3 is 2.51, which is very large, and the slope from T4 to T6 is 0.5, which is much smaller. This implies that the effect of conduction is dominant in the TEC section, and the effects of condensation and convection are dominant in the chamber section. Therefore, the average temperature of T4–T6 was used as the temperature $\overline{T}_c$ of the inner tube in the chamber.

The heat transfer coefficient and rate are obtained as follows: equation (1) is the conduction heat transfer equation for the TEC section.

$$Q_{e,\text{cond}} = k \cdot \frac{T_3 - T_1}{\Delta L_e} \cdot A_{\text{sec}}, \tag{1}$$

where $A_{\text{sec}} = \pi(R_o^2 - R_i^2)$.

According to the energy balance equation, the heat transfer rates owing to longitudinal conduction through the tube in the TEC section and through the tube in the chamber section are assumed to be the same as those in the following equation:

$$Q_{e,\text{cond}} = Q_{c,\text{cond}}. \tag{2}$$

The conduction heat transfer equation for a hollow cylinder was used to obtain the heat transfer rate via

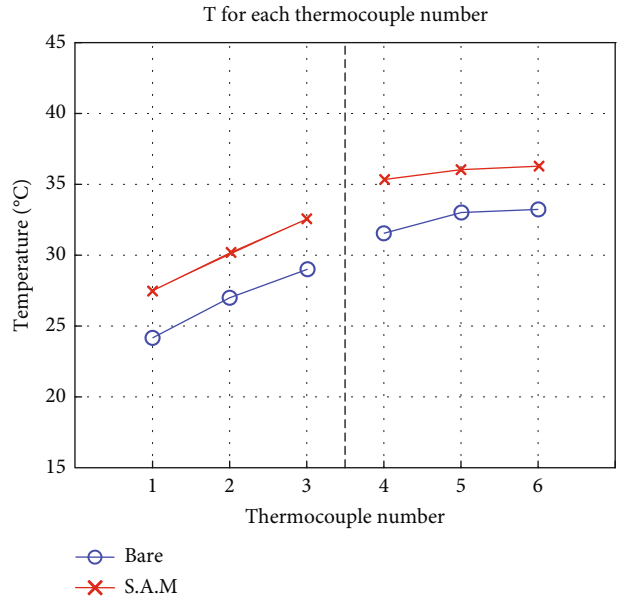

Figure 4: Temperature distribution of T1~T6 for bare and superhydrophobic tubes.

conduction in the chamber. The average outer surface temperature ($\bar{T}_s$) in the chamber was calculated using the following equation:

$$\bar{T}_s = \bar{T}_c - Q_{c,\text{cond}} * \frac{\ln\left(R_o/R_i\right)}{2\pi L_c k}. \tag{3}$$

According to the energy balance equation between condensation and convection in the tube inside the chamber and the longitudinal direction inside the chamber, equation (4) is valid.

$$Q_{c,\text{cond}} = Q_{c,\text{conv}}. \tag{4}$$

The condensation heat transfer coefficient (h) can be obtained by calculating $\bar{T}_s$. Equation (5) describes the condensation and convection heat transfers in the chamber.

$$Q_{c,\text{conv}} = h \cdot \left(\bar{T}_b - \bar{T}_s\right) \cdot A_{o,s}, \tag{5}$$

where $A_{o,s} = 2\pi R_o L_c$.

Using equation (6), the uncertainty in the heat transfer coefficient can be calculated. The errors in k, A, and Δx are negligible and therefore ignored.

$$\frac{\sigma_h}{h} = \sqrt{\left(\frac{\sigma_{Q_{c,\text{conv}}}}{Q_{c,\text{conv}}}\right)^2 + \frac{\sigma_{T_b}^2 + \sigma_{\bar{T}_s}^2}{\left(T_b - \bar{T}_s\right)^2}}, \tag{6}$$

where $\sigma_{Q_{c,\text{conv}}}/Q_{c,\text{conv}} = \sqrt{\left(\sigma_{T_1}/T_1\right)^2 + \left(\sigma_{T_3}/T_3\right)^2}$ and $\sigma_{\bar{T}_s}/\bar{T}_s = \sqrt{\left(\sigma_{T_4}/T_4\right)^2 + \left(\sigma_{T_5}/T_5\right)^2 + \left(\sigma_{T_6}/T_6\right)^2}$.

Finally, the uncertainties in the heat transfer coefficients of the bare and superhydrophobic tubes in the experimental results were less than 10.42%.

3. Results and Discussion

3.1. Heat Transfer Performance. Figure 5 shows the surface temperature of each tube. Five experiments were conducted using a bare tube, and three experiments were conducted using superhydrophobic tubes. The results were averaged and plotted along with standard deviations. The data for tube 5 were excluded from the analysis because of interference from the humid flow generated at the bottom of the chamber. The bulk fluid temperature difference between the superhydrophobic tubes and bare tubes was found to be a maximum of 2°C, and the bulk temperatures of the superhydrophobic tubes and bare tubes were very similar. As indicated in equation (5), the main variable that determines the difference in the heat transfer coefficients between the superhydrophobic and bare tubes is the difference between the bulk and surface temperatures. Therefore, because the bulk temperature difference is negligible, the main variable that determines the heat transfer coefficient is the surface temperature. Figure 5 shows that the surface temperature of the superhydrophobic tube is higher than that of the bare tube. Consequently, it was confirmed that

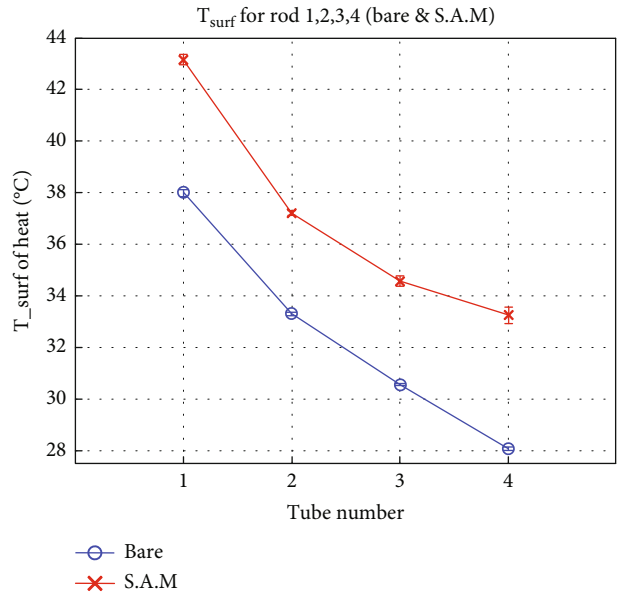

Figure 5: Comparison of surface temperatures of bare and superhydrophobic tubes.

the surface temperature of the superhydrophobic tube was higher than that of the bare tube by applying a superhydrophobic surface. Therefore, a high heat transfer coefficient value can be obtained with a smaller temperature difference between the bulk and surface temperatures in the superhydrophobic tube when it has a constant heat rate, as shown in equation (5).

Figure 6 illustrates the heat transfer rates, indicating that the superhydrophobic tube exhibited higher heat transfer rates than the bare tube across all tubes. Moreover, it can be observed that the heat transfer rate decreases from the top tube to the bottom tube. The upper tube exhibited a high heat transfer rate because it directly contacted humid air during condensation. Because the lower tube comes into contact with humid air after passing through the upper tube, heat transfer occurs with a smaller amount of humid air than in the upper tube, resulting in a low heat transfer rate. These results indicate that the heat transfer performance was significantly improved in the superhydrophobic tube compared to that in the bare tube. The heat transfer rate of the superhydrophobic tube in tube 1 increased by approximately 66% compared to that of the bare tube, whereas it increased by approximately 26% in tube 2, 22% in tube 3, and 25% in tube 4, indicating a consistent heat transfer performance improvement across all tubes.

Figure 7 shows the heat transfer coefficient according to the tube number. It can be observed that the heat transfer coefficient of the superhydrophobic tube is always higher than that of the bare tube in all cases, indicating that the SAM coating is effective in multiple-tube systems. Both the bare and superhydrophobic tubes exhibited the highest heat transfer coefficients in the second tube, suggesting that both condensation and convective heat transfer had a stronger effect on the second tube than on the first tube.

The difference in heat transfer coefficients between the second tube and other tubes in the bare tube system was

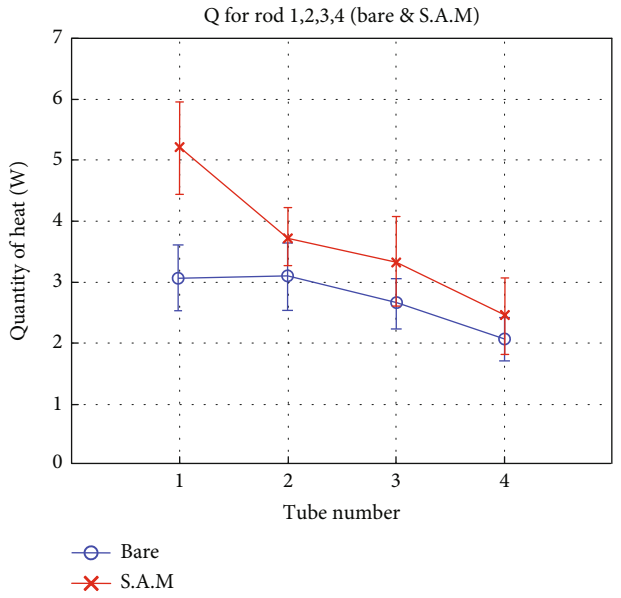

Figure 6: Bare and superhydrophobic tube heat transfer rate comparison.

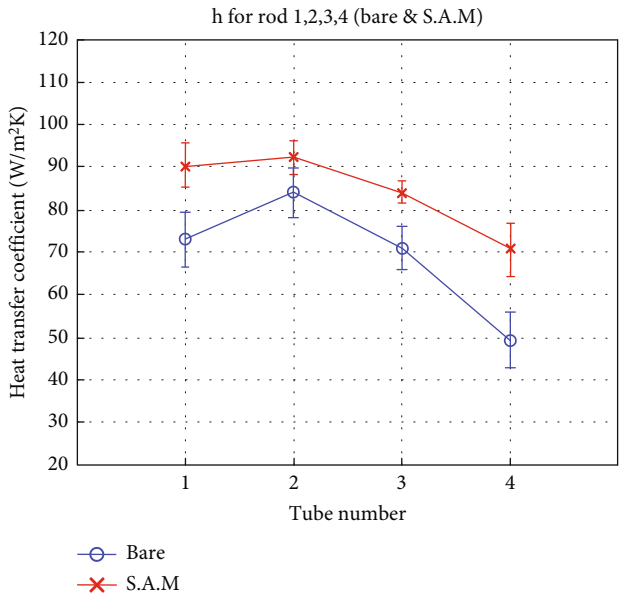

Figure 7: Bare and superhydrophobic tube heat transfer coefficient comparison.

13-66%, whereas in the superhydrophobic tube system, the difference was only 2-27%. This indicates that the effect of the condensation heat transfer was more significant in the superhydrophobic tube system than in the bare tube system. It should also be noted that the heat transfer coefficients improved by 9.5%–44.9% in all the superhydrophobic tubes.

3.2. Analysis of Droplet Dynamics. Figure 8(a) shows the droplets on the bare tube, and Figure 8(b) shows the droplets on the superhydrophobic tube. Looking at the blue boxes comparing the bottom of each tube, we can see that, in the case of the superhydrophobic tube, the surface area of the

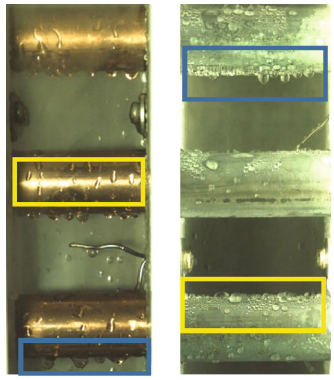

(a) Bare tube (b) SAM tube

Figure 8: Comparison of the shape of droplet of superhydrophobic tube and bare tube.

droplet in contact with the tube was small, and the contact angle was large. In addition, the droplet assumed a spherical shape. In contrast, the droplet on the bare tube had a larger surface area in contact and a smaller contact angle than the superhydrophobic tube, resulting in a bell-shaped droplet. This is because the surface energy of the superhydrophobic tube was lower than that of the bare tube, causing the droplets to coalesce more smoothly.

Looking at the yellow boxes comparing the tops of each tube, we can see that the size of the liquid droplet on the bare tube was generally larger than that on the superhydrophobic tube. This indicates that, in the case of the superhydrophobic tube, the droplet detached from the surface before it grew to a larger size, resulting in a shorter droplet growth period. The condensed shape of the droplets is also noteworthy. In the case of the superhydrophobic tube, the droplet assumes a nearly spherical shape similar to that at the bottom of the tube, whereas the droplet on the bare tube has a more oblong shape and is elongated vertically. This was because the droplet on the bare tube did not completely separate from the surface, causing it to adopt a more elongated shape. In contrast, the superhydrophobic tube completely refreshed the surface, allowing new droplet growth.

Figure 9 shows the moment at which a droplet detached from tube 1 of the bare tube influenced the droplet on tube 2 under normal operating conditions. As shown in Figure 9(a), when the droplet falls from the top tube, two thin water streams form on the surface of the intermediate tube. As shown in Figure 9(b), because a thin film had already formed on the intermediate tube, the droplet spread smoothly, resembling a saddle. As shown in Figure 9(c), as the saddle-shaped droplet flows downward owing to gravity, it merges with the water stream formed earlier, increasing the thickness of the water stream. The size of the droplets collected at the bottom of the tube also increased because of the influence of the droplets flowing on top of the intermediate tube. During condensation, the droplets spread widely, and the water stream remained.

Figure 10 shows the moment at which a droplet detaching from tube 2 of the superhydrophobic tube affected the droplet in tube 3 under normal conditions. Unlike the bare

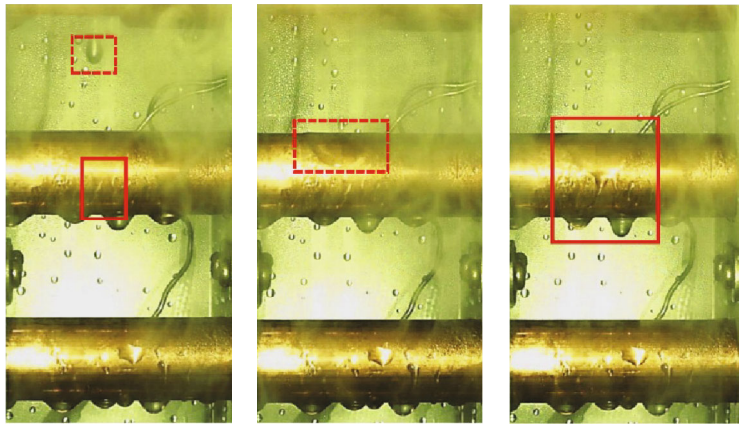

(a) 0.00 sec (b) 0.10 sec (c) 0.565 sec

Figure 9: Droplet dynamics of the flowing previous water stream shown with bare copper tubes (tube 1 to tube 3).

tube described earlier, the droplets in the superhydrophobic tube exhibited different dynamics. Figure 10(a) (i) shows a droplet falling from the upper tube. This droplet was smaller than the droplet in the bare tube and left a thin and distinct water stream. Figure 10(b) (ii) shows a droplet that leaves no water stream and only leaves a slight trace. Figure 10(b) (iii) shows the moment when the detached droplet merged with a preexisting droplet. Unlike the shape of the bare tube, it was confirmed that the droplet spreads less than that of the bare tube. This indicates that the droplets were better aggregated. When the aggregated droplets fell, the lumps fell together, leaving less water than in the bare tube. Such droplet dynamics were observed in all five superhydrophobic tubes. Therefore, it is expected that droplet condensation will continue under normal conditions.

Figure 10(c) (iv) shows the formation of a droplet as small droplets are absorbed during the merging of droplets flowing down the tube. When the droplet reached the bottom of the tube, small droplets remained as traces of passing droplets, as shown in Figure 10(d) (vi). Unlike the bare tubes, where the thickness of the remaining water film increased after the droplets flowed down the tube and left, the superhydrophobic tubes showed a slight residue of droplets due to surface renewal. As the droplets undergo further condensation, an increase in the frequency of surface renewal can significantly increase the frequency of the condensation process in all tubes, which affects the condensation heat transfer coefficient.

Figures 10(c) (v) and 10(d) (vii) show that as the droplets fall and sweep along the wider surface of the tube, surface renewal occurs, leading to an improved heat transfer efficiency in the tube. By contrast, in bare tubes, where film condensation occurs, the droplets must grow to a much larger size than the droplets in superhydrophobic tubes before they fall off the tube. Therefore, compared with Figure 9, it is evident that the frequency of surface renewal is much lower on the surface of the bare tubes.

Although the patterns of droplets falling from the tube varied, most of the droplet-falling behaviors were similar. To generalize the droplet-falling behavior, three cases can

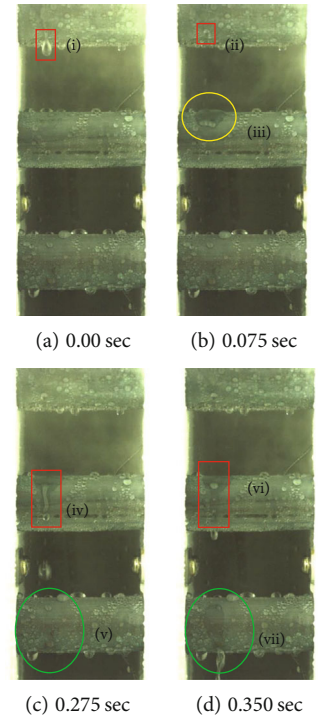

(a) 0.00 sec (b) 0.075 sec

(c) 0.275 sec (d) 0.350 sec

Figure 10: Droplet dynamics shown with superhydrophobic copper tubes (tube 2 to tube 4).

be considered: case 1: when droplets formed, they combined and fell to the lower end of the tube; case 2: droplets falling from the upper tube combine with the formed droplets and agglomerate at the lower end of the tube; and case 3: droplets falling from the upper tube combined with the formed droplets and fell before reaching the lower end of the tube. In case 3, there was a difference between the bare and superhydrophobic tubes. In the case of a bare tube, it is rare for a droplet to fall at an angle because there are many cases in which the droplet is transferred to the lower end of the tube along the water stream after falling. However, in the case of the superhydrophobic tube, most cases did not reach the lower end of the tube. Because the surface energy is low, the water stream

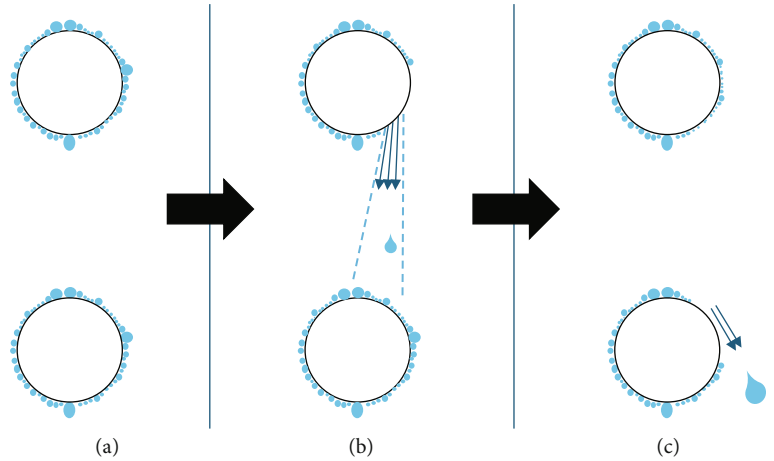

Figure 11: Droplet dynamics on superhydrophobic surfaces with multiple-tube interactions: (a) droplet condensation stage; (b) droplet falling stage; (c) droplet merging and falling stage.

is cut off, and it is more difficult to handle the number of falling droplets than in the bare tube. In this process, the surface of the lower tube was renewed and the droplet was repelled. This can occur even though the superhydrophobic tube is unaffected by the droplets falling from the upper tube.

Figure 11 shows the process for case 3. In Figure 11(a), it can be observed that condensation occurred first, and droplets formed on the tube surface. As shown in Figure 11(b), the droplet grew and fell, and the droplet size increased when the droplet renewed its surface. The droplets fell before reaching the bottom of the tube and landed at random locations. In Figure 11(c), the droplet falls on the side of the tube instead of on the lower end and combines with the droplet on the surface to fall. In other words, the superhydrophobic tube achieved surface renewal in case 3, which means that it had a positive effect on the heat transfer performance in multiple tubes.

4. Conclusion

The following are the results of the visualized humid condensation experiments performed on both bare and superhydrophobic horizontal copper tubes under atmospheric conditions. The condensation heat transfer performance was measured for each of the five copper tubes, and the droplet dynamics and evolution of the condensate droplets were observed for optical analysis using the TEC as a cooling device. It was found that continuous dropwise condensation, leading to frequent droplet sweeping, was successfully realized on the superhydrophobic-coated copper tubes and that the condensation heat transfer coefficient was enhanced for all tubes. The results were as follows:

(1) The heat transfer rate improved by 22%–66% on the superhydrophobic tube compared to that on the bare tube

(2) Furthermore, the heat transfer coefficient was observed to be higher on the superhydrophobic tube than on the bare tube for all sections, with an improvement of 9.5%–44.9%

(3) When condensation occurs on a bare tube, the droplet size is large, and the water stream continues to be present. In contrast, when condensation occurred on the superhydrophobic tube, the droplet size was relatively small, and a tendency to leave the droplet instead of creating a water stream was observed

(4) In addition, the bare tube had a higher droplet surface energy, resulting in a lower surface renewal frequency. However, the superhydrophobic tube has a lower droplet surface energy, resulting in a relatively higher surface renewal frequency

(5) It was confirmed that the droplets on the surface were more effectively removed when they fell from the superhydrophobic tube than from the bare tube. This implies that the heat transfer performance is further improved when interactions occur in multiple tubes

This research is mainly focused on normal atmospheric conditions with humid air and still allows the observation of the expected condensation process with a superhydrophobic surface, as the preparation of the superhydrophobic surface is deemed to be highly efficient and cost-effective, with great potential for real-world condensation applications. The application of superhydrophobic surfaces in multiple tubes is expected to be useful in actual condenser systems such as nuclear power plants.

Nomenclature

A: Area (m^2)
h: Heat transfer coefficient ($W/m^2 \cdot K$)
k: Thermal conductivity ($W/m \cdot K$)
L: Length (m)
Q: Heat transfer rate (W)
T: Temperature (°C)

$\bar{T}$: Average temperature (°C)
x: Distance (m)
R: Radius (m).

Subscripts

b: Bulk
c: Chamber
e: External chamber
i: Inner
o: Outer
sec: Cross-section
s: Surface
cond: Conduction
conv: Convection.

Data Availability

Data is available on request.

Conflicts of Interest

The authors declare that they have no known competing financial interests or personal relationships that could have appeared to influence the work reported in this paper.

Acknowledgments

This research was supported by the Basic Science Research Program through the National Research Foundation of Korea (NRF) funded by the Ministry of Education (RS-2023-00247899) and the Education and Research Promotion Program of KOREATECH in 2024.

References

[1] B. Khalil, J. Adamowski, A. Shabbir et al., "A review: dew water collection from radiative passive collectors to recent developments of active collectors," *Sustainable Water Resources Management*, vol. 2, no. 1, pp. 71–86, 2016.

[2] J. G. Qu, R. X. Tang, Q. Y. Cui, and J. F. Zhang, "Heat-transfer analysis of interfacial solar evaporation and effect of surface wettability on water condensation and collection," *International Journal of Thermal Sciences*, vol. 184, article 107911, 2023.

[3] S. Vemuri and K. J. Kim, "An experimental and theoretical study on the concept of dropwise condensation," *International Journal of Heat and Mass Transfer*, vol. 49, no. 3–4, pp. 649–657, 2006.

[4] J. W. Rose, "Dropwise condensation theory and experiment: a review," *Proceedings of the Institution of Mechanical Engineers, Part A: Journal of Power and Energy*, vol. 216, no. 2, pp. 115–128, 2002.

[5] X. Ma, J. W. Rose, D. Xu, J. Lin, and B. Wang, "Advances in dropwise condensation heat transfer: Chinese research," *Chemical Engineering Journal*, vol. 78, no. 2–3, pp. 87–93, 2000.

[6] M. Ahlers, A. Buck-Emden, and H.-J. Bart, "Is dropwise condensation feasible? A review on surface modifications for continuous dropwise condensation and a profitability analysis," *Journal of Advanced Research*, vol. 16, pp. 1–13, 2019.

[7] M. Azarifar, M. Budakli, A. M. Basol, and M. Arik, "On the individual droplet growth modeling and heat transfer analysis in dropwise condensation," *IEEE Transactions on Components, Packaging and Manufacturing Technology*, vol. 11, no. 10, pp. 1668–1678, 2021.

[8] E. J. Le Fevre and J. W. Rose, "An experimental study of heat transfer by dropwise condensation," *International Journal of Heat and Mass Transfer*, vol. 8, no. 8, pp. 1117–1133, 1965.

[9] R. Enright, N. Miljkovic, J. L. Alvarado, K. Kim, and J. W. Rose, "Dropwise condensation on micro- and nanostructured surfaces," *Nanoscale and Microscale Thermophysical Engineering*, vol. 18, no. 3, pp. 223–250, 2014.

[10] S. Najafpour, A. Moosavi, and H. Najafkhani, "Condensation enhancement on hydrophobic surfaces using electrophoretic method and hybrid paint coating," *Heat Transfer Engineering*, vol. 42, no. 18, pp. 1557–1572, 2021.

[11] C.-W. Lo, Y.-C. Chu, M.-H. Yen, and M.-C. Lu, "Enhancing condensation heat transfer on three-dimensional hybrid surfaces," *Joule*, vol. 3, no. 11, pp. 2806–2823, 2019.

[12] M. Budakli, T. K. Salem, and M. Arik, "An experimental and theoretical analysis of vapor-to-liquid phase change on micro-structured surfaces," *Applied Thermal Engineering*, vol. 178, article 115382, 2020.

[13] M. Budakli, T. K. Salem, M. Arik, B. Dönmez, and Y. Menceloglu, "An experimental study on the heat transfer and wettability characteristics of micro-structured surfaces during water vapor condensation under different pressure conditions," *International Communications in Heat and Mass Transfer*, vol. 120, article 105063, 2021.

[14] S. A. Khan, F. Tahir, A. A. B. Baloch, and M. Koc, "Review of micro–nanoscale surface coatings application for sustaining dropwise condensation," *Coatings*, vol. 9, no. 2, p. 117, 2019.

[15] J. T. Simpson, S. R. Hunter, and T. Aytug, "Superhydrophobic materials and coatings: a review," *Physical Society*, vol. 78, no. 8, article 086501, 2015.

[16] Q. Liao, Y. B. Gu, X. Zhu, H. Wang, and M. D. Xin, "Experimental investigation of dropwise condensation heat transfer on the surface with a surface energy gradient," *Journal of Enhanced Heat Transfer*, vol. 14, no. 3, pp. 243–256, 2007.

[17] M. H. Rausch, A. P. Fröba, and A. Leipertz, "Dropwise condensation heat transfer on ion implanted aluminum surfaces," *International Journal of Heat and Mass Transfer*, vol. 51, no. 5-6, pp. 1061–1070, 2008.

[18] N. Miljkovic, R. Enright, Y. Nam et al., "Jumping-droplet-enhanced condensation on scalable superhydrophobic nanostructured surfaces," *Nano Letters*, vol. 13, no. 1, pp. 179–187, 2013.

[19] S. Lee, K. Cheng, V. Palmre et al., "Heat transfer measurement during dropwise condensation using micro/nano-scale porous surface," *International Journal of Heat and Mass Transfer*, vol. 65, pp. 619–626, 2013.

[20] S. M. R. Razavi, J. Oh, R. T. Haasch et al., "Environment-friendly antibiofouling superhydrophobic coatings," *ACS Sustainable Chemistry & Engineering*, vol. 7, no. 17, pp. 14509–14520, 2019.

[21] A. Goswami, S. C. Pillai, and G. McGranaghan, "Surface modifications to enhance dropwise condensation," *Surfaces and Interfaces*, vol. 25, p. 101143, 2021.

[22] X. Ma, B. Tao, J. Chen, D. Xu, and J. Lin, "Dropwise condensation heat transfer of steam on a polytethefluoroethylene

film," *Journal of Thermal Science*, vol. 10, no. 3, pp. 247–253, 2001.

[23] M. Budakli, T. K. Salem, M. Arik, B. Donmez, and Y. Menceloglu, "Effect of polymer coating on vapor condensation heat transfer," *Journal of Heat Transfer*, vol. 142, no. 4, 2020.

[24] S. N. Aksan and J. W. Rose, "Dropwise condensation—the effect of thermal properties of the condenser material," *International Journal of Heat and Mass Transfer*, vol. 16, no. 2, pp. 461–467, 1973.

[25] I. O. Uçar and H. Y. Erbil, "Droplet condensation on polymer surfaces: a review," *Turkish Journal of Chemistry*, vol. 37, no. 4, p. 13, 2013.

[26] A. K. Das, H. P. Kilty, P. J. Marto, G. B. Andeen, and A. Kumar, "The use of an organic self-assembled monolayer coating to promote dropwise condensation of steam on horizontal tubes," *Journal of Heat Transfer*, vol. 122, no. 2, pp. 278–286, 2000.

[27] L. Chen, S. Liang, R. Yan, Y. Cheng, X. Huai, and S. Chen, "N-Octadecanethiol self-assembled monolayer coating with microscopic roughness for dropwise condensation of steam," *Journal of Thermal Science*, vol. 18, no. 2, pp. 160–165, 2009.

[28] M. R. Rajkumar, A. Praveen, R. Arun Krishnan, L. G. Asirvatham, and S. Wongwises, "Experimental study of condensation heat transfer on hydrophobic vertical tube," *International Journal of Heat and Mass Transfer*, vol. 120, pp. 305–315, 2018.

[29] F. Lv, S. Lin, H. Nie et al., "Droplet dynamics and heat transfer enhancement via dropwise condensation on helically-finned hydrophobic tube," *International Communications in Heat and Mass Transfer*, vol. 135, article 106153, 2022.

[30] N. Miljkovic and E. N. Wang, "Condensation heat transfer on superhydrophobic surfaces," *MRS Bulletin*, vol. 38, no. 5, pp. 397–406, 2013.

[31] M. M. Chen, "An analytical study of laminar film condensation: part 2—single and multiple horizontal tubes," *ASME Journal of Heat Transfer*, vol. 83, no. 1, pp. 55–60, 1961.

[32] A. Makas, *Condensation of steam on multiple horizontal tubes*, Master's thesis, Middle East Technical University, 2004.

[33] H. Ding, P. Xie, D. Ingham, L. Ma, and M. Pourkashanian, "Flow behaviour of drop and jet modes of a laminar falling film on horizontal tubes," *International Journal of Heat and Mass Transfer*, vol. 124, pp. 929–942, 2018.

[34] A. B. Kananeh, M. H. Rausch, A. Leipertz, and A. P. Fröba, "Dropwise condensation heat transfer on plasma-ion-implanted small horizontal tube bundles," *Heat Transfer Engineering*, vol. 31, no. 10, pp. 821–828, 2010.

[35] S. Liu, S. Shen, X. Mu, Y. Guo, and D. Yuan, "Experimental study on droplet flow of falling film between horizontal tubes," *International Journal of Multiphase Flow*, vol. 118, pp. 10–22, 2019.

[36] X. Zhu, S. Chen, S. Shen, S. Ni, X. Shi, and Q. Qiu, "Experimental study on the heat and mass transfer characteristics of air-water two-phase flow in an evaporative condenser with a horizontal elliptical tube bundle," *Applied Thermal Engineering*, vol. 168, p. 114825, 2020.

[37] H. W. Hu, G. H. Tang, and D. Niu, "Experimental investigation of convective condensation heat transfer on tube bundles with different surface wettability at large amount of noncondensable gas," *Applied Thermal Engineering*, vol. 100, pp. 699–707, 2016.

[38] X. WANG, S. YAN, Q. LIU, and Z. ZHU, "Experiment for drop-wise condensation heat transfer by infrared thermal imager," *Chinese Journal of Space Science*, vol. 36, no. 4, p. 520, 2016.

[39] A. Nakajima, "Design of hydrophobic surfaces for liquid droplet control," *NPG Asia Materials*, vol. 3, no. 5, pp. 49–56, 2011.

[40] N. D. Patil, R. Bhardwaj, and A. Sharma, "Droplet impact dynamics on micropillared hydrophobic surfaces," *Experimental Thermal and Fluid Science*, vol. 74, pp. 195–206, 2016.

[41] Y. Liu, L. Moevius, X. Xu, T. Qian, J. M. Yeomans, and Z. Wang, "Pancake bouncing on superhydrophobic surfaces," *Nature Physics*, vol. 10, no. 7, pp. 515–519, 2014.

[42] J.-W. Lee, D. Y. Ji, K. Y. Lee, and W. Hwang, "A study of droplet-behavior transition on superhydrophobic surfaces for efficiency enhancement of condensation heat transfer," *ACS Omega*, vol. 5, no. 43, pp. 27880–27885, 2020.

[43] X. Wang, B. Xu, Z. Chen et al., "Review of droplet dynamics and dropwise condensation enhancement: theory, experiments and applications," *Advances in Colloid and Interface Science*, vol. 305, article 102684, 2022.

[44] E. Celia, T. Darmanin, E. Taffin de Givenchy, S. Amigoni, and F. Guittard, "Recent advances in designing superhydrophobic surfaces," *Journal of Colloid and Interface Science*, vol. 402, pp. 1–18, 2013.

[45] Y. Zhong, A. M. Jacobi, and J. G. Georgiadis, *Condensation and wetting behavior on surfaces with micro-structures: superhydrophobic and super-hydrophilic*, Purdue e-Pubs, 2006.

[46] A. W. Neumann, A. H. Abdelmessih, and A. Hameed, "The role of contact angles and contact angle hysteresis in dropwise condensation heat transfer," *International Journal of Heat and Mass Transfer*, vol. 21, no. 7, pp. 947–953, 1978.